The Global Zonally Integrated Ocean Circulation, 1992–2006: Seasonal and Decadal Variability

CARL WUNSCH AND PATRICK HEIMBACH

Department of Earth, Atmospheric and Planetary Sciences, Massachusetts Institute of Technology, Cambridge, Massachusetts

(Manuscript received 11 March 2008, in final form 20 August 2008)

ABSTRACT

The zonally integrated meridional and vertical velocities as well as the enthalpy transports and fluxes in a least squares adjusted general circulation model are used to estimate the top-to-bottom oceanic meridional overturning circulation (MOC) and its variability from 1992 to 2006. A variety of simple theories all produce time scales suggesting that the mid- and high-latitude oceans should respond to atmospheric driving only over several decades. In practice, little change is seen in the MOC and associated heat transport except very close to the sea surface, at depth near the equator, and in parts of the Southern Ocean. Variability in meridional transports in both volume and enthalpy is dominated by the annual cycle and secondarily by the semiannual cycle, particularly in the Southern Ocean. On time scales longer than a year, the solution exhibits small trends with complicated global spatial patterns. Apart from a net uptake of heat from the atmosphere (forced by the NCEP–NCAR reanalysis, which produces net ocean heating), the origins of the meridional transport trends are not distinguishable and are likely a combination of model disequilibrium, shifts in the observing system, other trends (real or artificial) in the meteorological fields, and/or true oceanic secularities. None of the results, however, supports an inference of oceanic circulation shifts taking the system out of the range in which changes are more than small perturbations. That the oceanic observations do not conflict with an apparent excess heat uptake from the atmosphere implies a continued undersampling of the global ocean, even in the upper layers.

1. Introduction

The North Atlantic meridional overturning circulation (NA-MOC) has been the focus of intense interest, in part because of widely publicized claims that it controls much of the climate system and/or is in imminent danger of ''collapse.'' A number of studies (e.g., Hurrell et al. 2006) have discussed predicting the NA-MOC under the presumption that it is a dominant component of ongoing climate change. Wunsch and Heimbach (2006), using the great majority of global data and a general circulation model (GCM), described the behavior of the MOC in the Atlantic at 25°N between 1993 and 2004, concluding that there were apparent weak trends of changing signs at various depths in the meridional volume transport but that there was no evidence for a significant trend in the enthalpy (temperature) transport.

But climate is global, and the NA-MOC is a small part of the ocean circulation that can only be understood in the wider context. Here we examine the planetary zonally integrated meridional ocean circulation as computed from a combined oceanic GCM and the large datasets in the Estimating the Circulation and Climate of the Ocean (ECCO)–Global Ocean Data Assimilation Experiment (GODAE) estimates [see Wunsch and Heimbach (2007) for a complete description] and analyze its mean and variability over the 14-yr period 1992–2006, with emphasis on the GODAE estimates. There are no eddies present in this 1° horizontal, 23-vertical layer representation and thus the variability is a lower bound (e.g., Wunsch 2008). The specific solution is denoted v3.35 and differs quantitatively in numerous ways from the unoptimized control run (v3.0) that represented the starting estimate. A brief description of the v3.35 ECCO–GODAE estimate is that it is the result of a least squares fit of a GCM to a global, weighted dataset, 1992–2006. Comparisons (not shown) of the equivalent results in the ''control'' solution obtained by forcing the Massachusetts Institute of Technology GCM

Corresponding author address: Carl Wunsch, Department of Earth, Atmospheric and Planetary Sciences, Massachusetts Institute of Technology, Cambridge, MA 02139.
E-mail: cwunsch@mit.edu

DOI: 10.1175/2008JPO4012.1

(MITgcm) with the unmodified National Centers for Environmental Prediction–National Center for Atmospheric Research (NCEP–NCAR) reanalysis in the configuration discussed by P. Heimbach (2008, unpublished manuscript) lead to the inference that changes in the circulation required by the optimization are quantitative rather than qualitative, the variability structure remaining largely the same. An exception to this statement is that the mean Atlantic MOC is qualitatively shifted in magnitude. Similar comparisons (not shown) to earlier near-optimized solutions (v2.216 and v3.22) display nearly indistinguishable results, supporting the inference of a now stable estimate.

Readers unfamiliar with the details of the ECCO–GODAE methods need only be aware that the estimates used here are computed from a *freely running* forward model, whose initial–boundary conditions have been adjusted by least squares so that the model comes as close as practical to the data within estimated error estimates: unlike some other approaches, the resulting solution satisfies the model equations exactly. In particular, the estimation procedure does not introduce any spurious sources or sinks of any field.

Discussion of almost any aspect of the global ocean circulation runs the risk of extending to book length. The shorthand ''MOC'' is convenient, but fundamentally we are examining the zonal projection of a three-dimensional flow field. Use of zonally integrated quantities in geographical coordinates has the advantage of simplifying the results and making their display reasonably straightforward. It has the disadvantage of precluding analysis of the three-dimensional flow and transport fields producing the integrated results—no two-dimensional projection describes a three-dimensional flow. Seeming paradoxes can arise from such projections if they are interpreted as representing particle pathways. These disadvantages are set aside for the time being in an effort to produce a comprehensible, simple description of the ocean circulation variability—a form of description that has been widely invoked to discuss present, past, and future climate states. Recalculation of the results in, for example, neutral density space in the Southern Ocean, and in stream-coordinates as the residual mean, would be illuminating, but again these are not displayed here. In our present usage, MOC refers to the top-to-bottom circulation; some other authors employ the term for the very-near-surface, highly volatile flow, which for purposes of this paper is regarded as a nearly separate subject.

Before analyzing the estimated results, it is useful to recall the venerable (Veronis and Stommel 1956) and well-supported theory (Gill 1982; Pedlosky 2003; Cessi et al. 2004) of large-scale ocean response to relatively small disturbances. One expects the baroclinic open ocean to be governed in large part by the zonal propagation of signals by baroclinic Rossby waves. At midlatitudes, the group velocity of such a wave requires on the order of a decade to propagate a signal across a 5000-km-wide ocean, with the time growing substantially at higher latitudes (see also Anderson and Corry 1985; Sturges et al. 1998). The inability of the subtropical and higher-latitude oceans to respond baroclinically at annual periods is the basis of the Gill and Niiler (1973) depiction of the seasonal variability as essentially local except at low latitudes, an inference that has stood the test of time. (Barotropic adjustment is much faster but only affects the temperature and salinity structure in an indirect manner.)

Figure 1 displays the approximate time required for the baroclinic Rossby wave with the fastest group velocity to cross a 5000-km-wide ocean as a function of latitude. The fastest wave is, in the basic theory, the one with the basin-scale wavelength. The multidecadal time scale in the modeling results of Cessi et al. (2004) is fully consistent with expectation. These times (and basin widths do shrink with latitude) are *not* the adjustment time—they are the shortest time over which large-scale baroclinic adjustment can be expected to *start*.[1] Such times are the result of linear perturbation theory and would not necessarily be applicable in a situation in which the ocean was subject to a major finite amplitude disturbance. A question raised below is whether there is any evidence that the ocean is, in modern times, being subjected to such large disturbances that the simple theory is rendered invalid. Anticipating the conclusions, results are consistent with the rough temporal scaling argument embodied in Fig. 1 and the inference that over the last 15 yr, disturbances lie well within the perturbation range. The Southern Ocean is a partial exception to the conclusions about time scales—presumably because its strong barotropic response interacts effectively with the complex topography there.

Convective injection of surface waters into the abyss at high latitudes might be thought to short-circuit the baroclinic wave adjustment time. Consider, however, that convective regions are by nature extremely small, and although communication between surface and abyss is locally fast, the ability to adjust large fractions of the abyssal ocean will again depend on the wave-signal velocities, or even slower advective ones carrying information away from the convective area. By way of

[1] Baroclinic Kelvin waves—coastal and equatorial—are much faster, but they influence the ocean interior only indirectly through their coupling to Rossby waves when reflecting and/or shifting latitude.

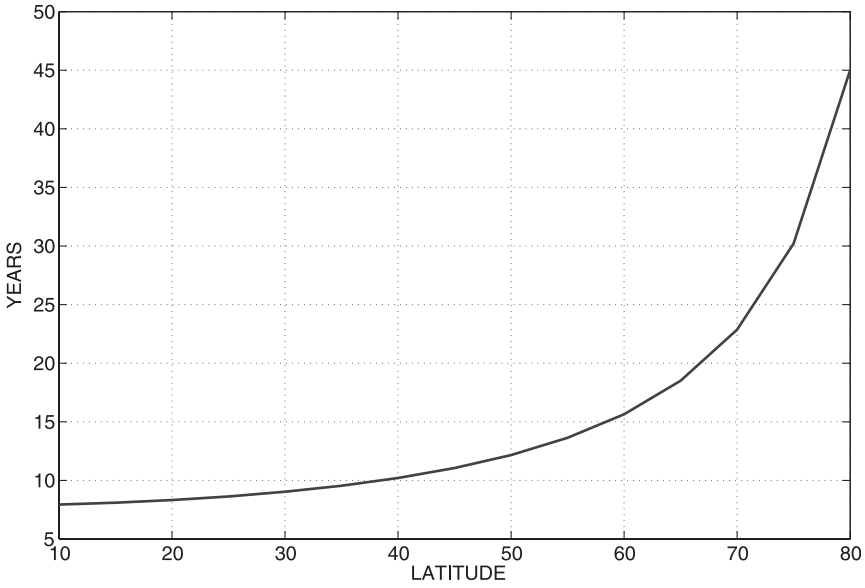

FIG. 1. Time for a disturbance traveling with the group velocity of a Rossby wave of wavelength $L = 5000$ km to cross a basin of width L (shorter waves can take much longer). A fixed Rossby radius of 30 km was used; only β was permitted to change with latitude. [See Veronis and Stommel (1956), although here a continuously layered ocean was used rather than their two layers.] At high latitudes, decades are required to begin the adjustment process, even accounting for basin narrowing and the large changes in deformation radius. Final equilibrium requires much more time.

example, notice that the North Atlantic volume between 50° and 80°N is about 1.5×10^{16} m^3. If the change in convective injection of surface water were as large as 10 Sv (an extremely large value; 1 Sv $\equiv 10^6$ m^3 s^{-1}), and if the entire convected volume were restricted to that region (physically impossible), then the time to replace the water mass would be about 50 yr. *Basin-wide baroclinic variability in the deep oceans on a decadal time scale is not expected*—with implications both for predictability and near-term detectability. Coarse-resolution models that do apparently produce major, deep, baroclinic open ocean adjustments on subdecadal time scales have a numerical physics in need of close scrutiny.

Consider yet another rough scale analysis. Oceanic potential energy (PE) is

$$\mathrm{PE} = \int\int\int_{-\eta(\lambda,\phi)}^{\eta(\lambda,\phi)} zg\rho(\lambda,\phi,z)dzdA,$$

with g being gravity, ρ density, ϕ latitude, λ longitude, z the vertical coordinate, dA the area differential, h the depth, and η the sea surface elevation. In a linear approximation, $\rho = \rho_0(1 - \alpha T + \beta S)$, with T being temperature, S salinity, and $\rho_0 \approx 1029$ kg m^{-3}. Estimates of energy transfer rates to the ocean circulation from the atmosphere are today on the order of 1 TW (10^{12} W). Keeping everything else fixed, let us suppose, to derive a time scale, that the ocean below 1000 m undergoes a temperature change (either sign) of 1°C. Then,

$$|\Delta \mathrm{PE}| \approx \left| g\rho_0 \int\int\int_{-h(\lambda,\phi)}^{-1000\mathrm{m}} (-\alpha \Delta T) z dz dA \right| \approx 10^{22}\mathrm{J}$$

(using $\alpha \approx 1.7 \times 10^{-4}$ °C^{-1} and $h \approx -4000$ m).

Cooling of the abyss lowers the center of mass and implies a reduction in PE that could be released as kinetic energy (KE) or transferred through the sea surface; correspondingly, a warming represents an increase in PE, which could derive from mixing forced by oceanic kinetic energy or again by transfer across the sea surface. If the modern power input on the order of 1 TW were to be disturbed by 100%, then it would take about 300 yr to bring about an energy shift of this magnitude. [Estimated modern conversion rates between PE and KE are less than 1 TW; see Ferrari and Wunsch (2009).] Qualitative shifts in the circulation potential energy would require *multi decadal* periods unless the energy transfer rates both within the ocean and to and from the atmosphere were greatly modified from present-day value—implying a significant shift in the way existing air–sea coupling or interior mixing occurs. Corresponding changes in internal and kinetic energy are being ignored here. Equivalent calculations can be made for salinity (freshwater input) changes.

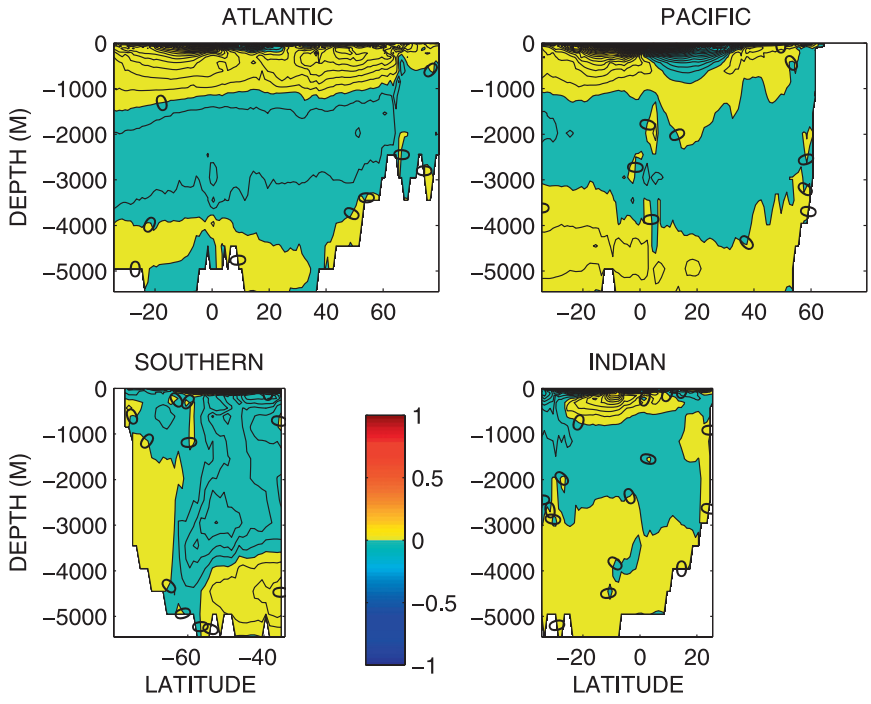

FIG. 2. Mean (1992–2006) of the meridional volume flux (Sv m^{-1}) from ECCO–GODAE v3.35. Yellow areas are northward moving; blue-green, southward. Note the complex equatorial structure in the Atlantic and Pacific. Contour interval is 0.005 Sv m^{-1}. In the Southern Ocean, the interpretation of zonally integrated Eulerian means requires particular care owing to the complex topography and relatively important eddy transport field. The near-equatorial structure at depths is seen to be much more complex when a tighter contour interval is used than the one here.

Conventionally, the MOC is displayed as a streamfunction in latitude and vertical coordinates (ϕ and z, respectively; see, e.g., Talley 2003; Lumpkin and Speer 2007), but because the human eye is poorly adapted to taking spatial derivatives, that representation is less visually informative than one in the two components v and w of the Eulerian velocities. Thus, for each ocean basin, including the Southern, the meridional velocity v is integrated zonally to produce, for example, $V_i(\phi,z,t)$, where i is used to denote the results in each of the four basins (Atlantic, Pacific, Indian, and Southern) and time means $\overline{V}_i(\phi, z)$ and $\overline{W}_i(\phi, z)$ are formed. Another advantage of using v, w is that the Indian and Pacific Oceans can be depicted independently, whereas the use of a streamfunction would require the summation of those basins. The model is defined at 1° intervals of latitude and longitude, between 79.5° north and south, and in 23 levels,[2] so that $\phi = \phi_j$ and $z = z_k$ corresponding to integer values j, k (with k defining the center of the layers). For context, we begin with a brief description of the time means, turning later to the variability. Ocean dynamics depend most directly on the mass (volume) flux, whereas the coupled atmosphere responds most immediately to the enthalpy (heat) transport and, particularly, the related sea surface temperature. Oceanic freshwater transport is also important, but in the interests of restricting the length of this discussion, we here omit any discussion of freshwater and salinity.

2. Mean global volume and enthalpy (heat) transports

a. Volume transport

Some of the time-mean transports involved in the global MOC are displayed here to provide the context for examination of their variability. Figure 2 displays $\overline{V}_i(\phi, z)$, over the entire 15 yr, for the Atlantic, Pacific, and Indian Oceans (all north of 38°S) as well as for the Southern Ocean. In terms of volume, the Pacific and Indo-Pacific Oceans are the dominant element of the

[2] Layer interfaces are at 0, 10, 20, 35, 55, 75, 100, 135, 185, 260, 360, 510, 710, 985, 1335, 1750, 2200, 2700, 3200, 3700, 4200, 4700, 5200, and 5700 m.

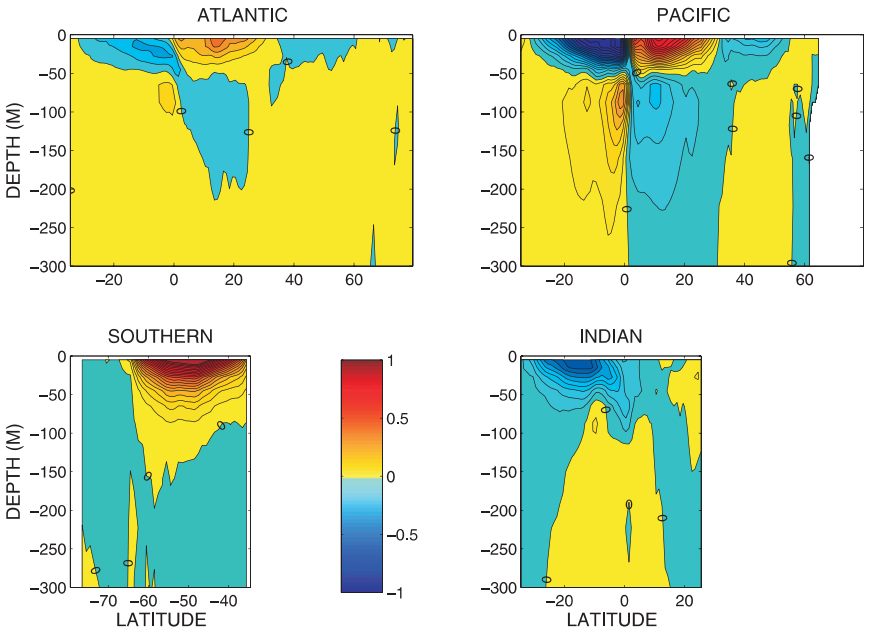

FIG. 3. As in Fig. 2, but only for the upper 300 m. Notice in particular the complex structure at and near the equator.

MOC. Ganachaud (2003) provided independent estimates of the zonal integrals at a few latitudes in the global ocean. In gross terms, one sees an Atlantic with a conventional MOC, having a (net) northward flow in the upper approximately 1000 m, a southward flow between about 1000 and 4000 m, and a generally northward flow again below that. The color shifts across fixed depths imply vertical divergences necessary to conserve volume or mass. (The reader is reminded that all of these net flows are residual sums of complicated zonally and temporally varying Eulerian velocities.)

The Pacific circulation is also as expected, with a surface outcropping of the southward flow in the Northern Hemisphere consistent with intermediate water formation and penetration of water from the circumpolar area near surface and bottom, sandwiching a southward return

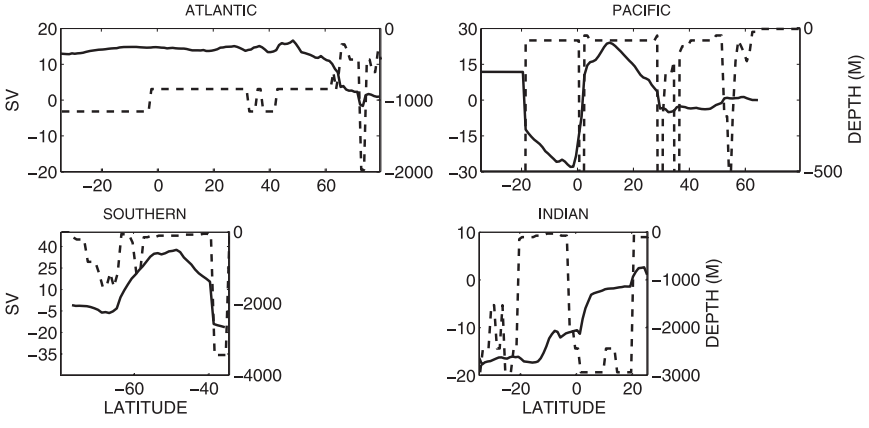

FIG. 4. Maximum meridional volume transport values (Sv), irrespective of sign for the time mean in each basin (solid curve, left axis) and the depth (dashed curve, right axis) to which one must integrate to achieve the maximum. Note the truncated depth scale used for the Pacific. The very stable value of the maximum transport in the Pacific south of 20°S appears to be a coincidence (and the value is not strictly constant). Note that the Pacific and Indian Oceans are connected so that they individually can have a net (top to bottom) in or outflow that does not vanish. The off-scale Pacific depth lies near the bottom.

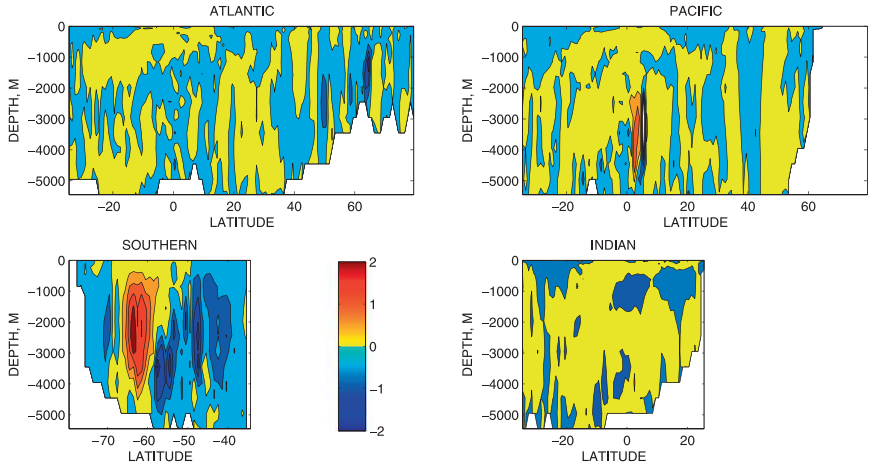

FIG. 5. The quantity $\overline{W}(\phi, z,)$, the zonally summed time-mean vertical velocity W in hundredths of Sv (no normalization by layer thickness), at intervals of 0.05×10^{-3} Sv. Patterns are complex and difficult to summarize. In the North Atlantic, the strong downwelling near 65°N is close to but not the same as the region of convection (see Scott and Marotzke 2002). A conspicuous Deacon cell appears in the Southern Ocean, but the reader is reminded of the caveat not to interpret two-dimensional time-averaged projections of Eulerian mean velocities as corresponding to particle velocities. Streamfunction representations imply these complicated vertical velocities, but taking visual derivatives is difficult. The boundary between the yellow (upward) and blue (downward) regions is the zero line of the vertical motion.

flow at intermediate depths. The less familiar Indian Ocean is similar on average to the South Pacific. Dynamically, and also unsurprisingly, the Southern Ocean is quite different from the others, with intense meridional flow appearing only below the sill depths; it is dominated by inflow from the north, with strong northward flow being confined to great depths at lower latitudes. An intricate cellular structure appears at depth on the equator in the Atlantic and Pacific Ocean, particularly in the latter. Results from the control run, v3.0, are grossly similar but differ in many details.

Figure 2 is a bit misleading in that the near-surface (and near-bottom) flows are quite intricate, as can be seen in Fig. 3, which is identical to Fig. 2 except for showing an expanded upper 300 m. The Pacific result has a strong qualitative resemblance between 8°S and 10°N to Fig. 5a of Johnson et al. (2001), who used shipboard ADCP data, not employed here, in displaying the near-surface divergence expected from Ekman layers, overlying a reversed sense flow below that to about 300 m, with southward flow to about 100 m on the equator itself. The Atlantic shows a similar but weaker structure. A more detailed discussion of the near-equatorial physics would, however, take us too far afield from a global account. The near-surface Southern Ocean displays a divergence about, very roughly, the mean latitude of the Antarctic Circumpolar Current, with a strong equatorward Eulerian mean to the north of the axis—again as one would anticipate from Ekman theory. (The eddy volume flux must be accounted for there, should one seek to discuss particle motions.)

Much attention has gone toward determining the poleward volume flux; Fig. 4 displays the maximum definable value (whether poleward or equatorward), obtained by integrating downward from the surface, in each ocean basin. Atlantic values near 15 Sv are conventional. The control differs qualitatively in the Atlantic, for example, where in that solution the maximum meridional overturning increases with latitude from little more than 12 Sv to more than 23 Sv by about 50°N. For this component, the optimization has made an important change. Although often ignored, the enormous mass of water in the Pacific and Indian Oceans produces maximum meridional transports that are at least as large as those in the North Atlantic, although the low-latitude tropical Pacific circulation is concentrated at near-surface depths where Ekman fluxes are very large.

The vertical velocities associated with the divergences of the meridional flow in Fig. 2 are shown in Fig. 5. It is these structures that are so difficult to perceive in streamfunction plots. The patterns are not globally simple, but a number of familiar features do emerge, including the comparatively strong near-surface equatorial upwelling, a strong Deacon cell in the Southern Ocean, and a strong downwelling in the high-latitude convective region of the North Atlantic. [See Scott and Marotzke (2002) for a discussion of vertical velocities and convective mixing in idealized models.]

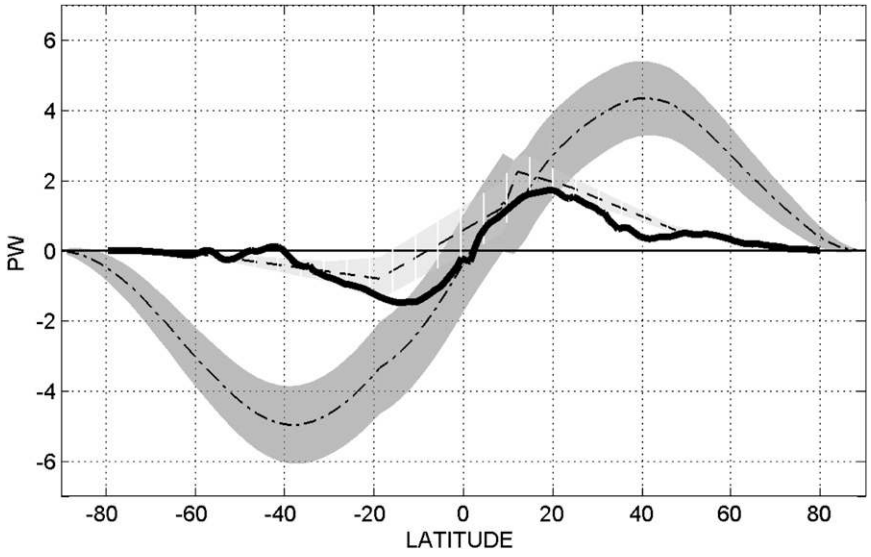

FIG. 6. Estimate with 1σ error bars (gray shading) of the ocean (dashed) and atmospheric (dashed–dotted) meridional enthalpy fluxes (adapted from Wunsch 2005, primarily from results of Ganachaud and Wunsch 2003). The major inference is that poleward of about 50° in both hemispheres, the mean oceanic component is very small, and hence little variability in its values would be expected or is seen. Although the hydrographic sections used to make the estimates are also part of the ECCO–GODAE datasets, the model used by Ganachaud and Wunsch (2003) is a very different one from the GCM. Atmospheric values were computed as a residual of the ocean circulation transports subtracted from earth radiation budget values. That the changing MOC at high latitudes is a major cause of climate change, other than regionally, is implausible given the minute contribution the ocean makes to the meridional heat transport there. The heavy black line is taken from Fig. 7 and is the estimate made from v3.35. Within two standard errors, the result is everywhere consistent with the direct oceanic estimate.

The flow pathways dictated by these time means are not our present focus. Nonetheless, some understanding of the basic time-averaged pathways can be obtained from the long-term tracer experiments of Wunsch and Heimbach (2008) and/or the schematic of Lumpkin and Speer (2007), which appears qualitatively plausible.

b. Enthalpy transport

MOCs exist of volume, temperature (approximately enthalpy or heat), freshwater, oxygen, nutrients, and so on, and none are identical because the integrals involved in computing the zonal transports involve differing covariances of the time and zonally varying velocities and scalar properties. Vertically integrated temperature transports and their divergences are uniquely determined in a mass conserving system. Analogs of Fig. 2 for temperature movements are, as expected, greatly surface intensified and closely resemble the volume transport maps. But because, as a reviewer has emphasized, one can arbitrarily shift the temperature zero, their form is nonunique (taking the temperature zero near 25°C would, for example, greatly emphasize the abyssal circulation). A more (nearly) unique representation can be obtained, for example, by following Boccaletti et al. (2005) in computing a ''heat function'' whose along streamfunction temperature transport vanishes (equivalent to suppressing any nondivergent transport). In a three-dimensional time-varying flow field as here, such a calculation is quite onerous if done accurately and so is omitted. But because the divergences to the atmosphere remain unique, the net enthalpy flux and its variations can be estimated.

Interpretation of the enthalpy (heat) transport variability requires a context of the magnitudes of the time-mean transports. Figure 6 shows an estimate of the oceanic meridional heat transport (Wunsch 2005) computed independently of the ECCO–GODAE estimates (primarily from Ganachaud and Wunsch 2003). For comparison, the ECCO–GODAE result is shown in Fig. 7 and with the global sum plotted again on Fig. 6. Within error estimates, the global totals from the two estimates are indistinguishable, although the ECCO result is closer to antisymmetry about the equator. Because of the strong eddy transport in the Southern Ocean, the value shown there differs qualitatively from those obtained from an eddy-permitting model (Mazloff

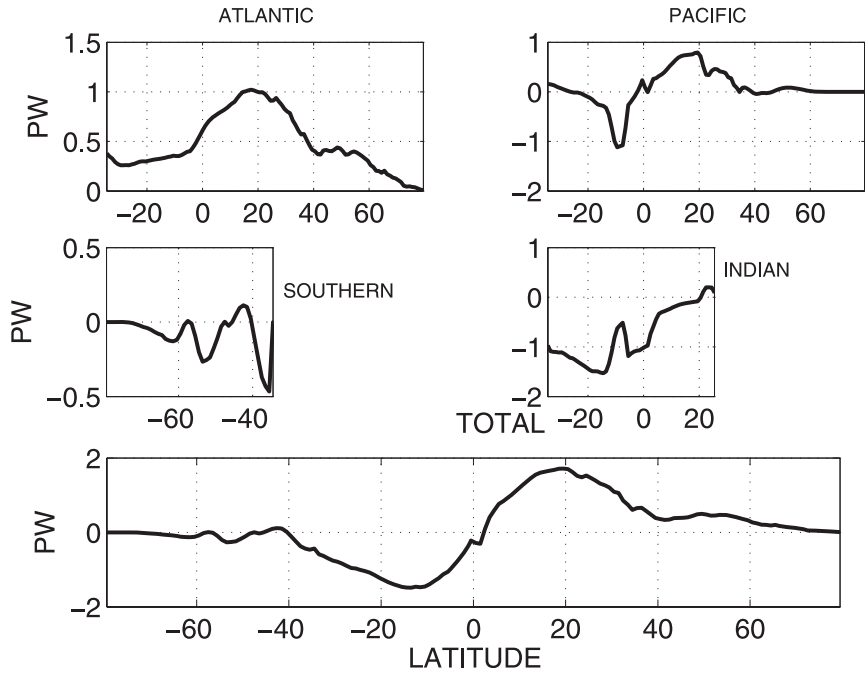

FIG. 7. Total enthalpy transport (PW) in each basin and the global total from ECCO–GODAE v3.35. The total (lowest panel) does not show as great an antisymmetry as seen in the ocean estimate in Fig. 6, but the estimates are consistent within the error bars of that figure alone, without consideration of the uncertainty of the model itself. (The total is also plotted in Fig. 6.)

2008) or in the residual mean computed from the present model. In Mazloff's results, the eddy contribution is such as to remove much of the structure seen in Fig. 7, leading to a nearly linear increase in the total southward heat transport from south to north reaching about −0.4 PW at the northern limit.

3. Global variability

Figure 8 depicts the variance of $V(\phi,z,t)$ over 15 yr in the solution (the global standard deviation of the variability is 1.2 Sv). Most of the variance at depth is, as expected, at low latitudes, with the exception of the deep Southern Ocean in the region of topographic structures. Much of the variability is confined to the very upper layers of the ocean, within less than 300 m of the sea surface, and fluctuates in response to the changing wind and buoyancy exchanges. Of that variability, the great majority (with one exception taken up below) is dominated by the annual cycle and, secondarily, the semiannual one. The annual cycle has been the subject of much separate study [see particularly the review by Jayne and Marotzke (2001); in the ECCO–GODAE context, see Vinogradov et al. (2008)] and is not our focus, which is the behavior of the great mass of ocean volume lying below these surface layers. Nonetheless, because it proves surprisingly important even below the surface, it has to be touched upon in the analysis below. A fuller discussion of the behavior of the ECCO–GODAE solutions in close proximity to the sea surface will be provided elsewhere. Deep Southern Ocean changes are dominated by a semiannual component. See Webb and de Cuevas (2007) and Olbers and Lettmann (2007) for discussion of the variability of the Southern Ocean, which has a powerful barotropic component as compared to the other oceans.

a. Volume transport components

The analysis procedure is a standard one for empirical orthogonal functions (EOFs; e.g., Jolliffe 2002; von Storch and Zwiers 1999), although we prefer a slightly unconventional description using the singular value decomposition (see the appendix). For each basin, a monthly anomaly of meridional transport is computed as $V_i'(\phi_j, z_k, t_p) = V_i(\phi_j, z_k, t_p) - \overline{V}_i(\phi_j, z_k)$ and the spatial EOFs, here called $\mathbf{u}_i$, are computed with temporal coefficients $\mathbf{v}_i(t)$ and a singular value λ_i. As is always the case with EOFs, a decision about weighting has to be made; the fields could be given uniform variance or normalized to represent zonal averages rather than integrals. Here the raw, volume-weighted integrals represent the variables with the most immediate impact on

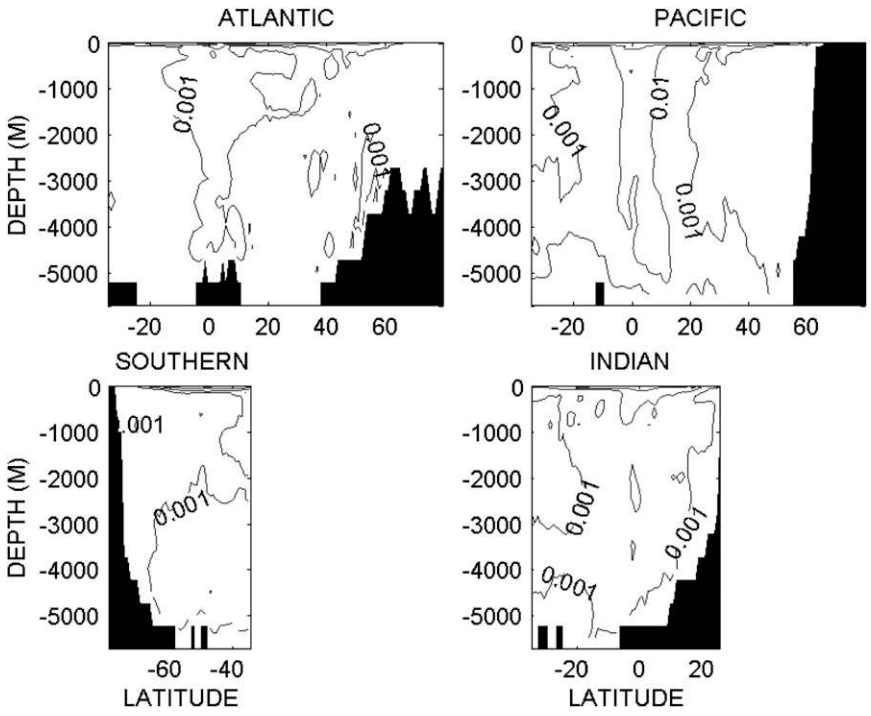

FIG. 8. Temporal variance from monthly means in the v3.35 solution of $V(\phi,z,t)$ in Sv. Values are first divided by the layer thickness and then by the total variance [$(1.2\ \text{Sv})^2$] prior to plotting. Contour interval is logarithmic, starting as 0.001, 0.01,.... As the theory in Fig. 1 implies, the system is dominated by fluctuations at low latitudes over decadal time scales, with little relative variability expected or seen at high latitudes. Southern Ocean excess variance at depth is likely associated with the special dynamics of the topographic interactions there at those depths driven by a forceful barotropic field. The great mass of the Pacific Ocean dominates, particularly in the equatorial band.

the climate system; the resulting heavy weighting of the Pacific and Southern Oceans represents their enormous mass of fluid that at zero order will control the air–sea transfer processes. Other weightings will produce results that differ, and their analysis likely would be enlightening. In displaying the results, the spatial patterns of $\overline{V}$ and other transports have been divided by the layer thicknesses to avoid giving undue visual weight to the numerical values in the thick abyssal ones.

EOFs capture the dominant correlation structures in spatially or temporally varying fields. The simple theoretical framework and 15-yr time interval here provides little scope for signal propagation and hence development of strong covariances within the ocean from its internal dynamics. To the degree that correlations are found (and they are), one anticipates at the outset that they will largely be atmospheric-forced structures with a global reach, rather than reflecting internal oceanic dynamics. Barotropic modes in the ocean are an exception to the expectation of little global-scale dynamical response within 15 yr, but these appear to have only marginal impacts on the thermal and salinity structures of the ocean and little sign of their importance to climate change can be detected here. El Niño–Southern Oscillation (ENSO) signals do become apparent and are a combination of regional (tropical) and atmospherically induced (nontropical) change.

The issue of trends and drifts is one of the more difficult ones involved in using GCMs, and we postpone that discussion. For the moment, note only that some but by no means all of the $\mathbf{v}_i(t)$ display starting transients ranging from a few months to 2+ years. The effect is particularly pronounced in the Atlantic basin; in particular, for the spectral results shown below, the first 2 yr of the estimates were dropped in the Fourier analysis used to calculate power density estimates. These starting transients are generally not present in the control (v3.0) and are thus not simple spin-up contributions.

Figures 9 and 10 display the first two singular vectors (EOFs) of the volume flux containing, respectively, 43% and 8% of the total volume variability of $(1.2\ \text{Sv})^2$. As with all EOFs here, they are computed globally, reflecting the largest scale covariances, but are displayed by ocean basin for interpretation. Many more vectors

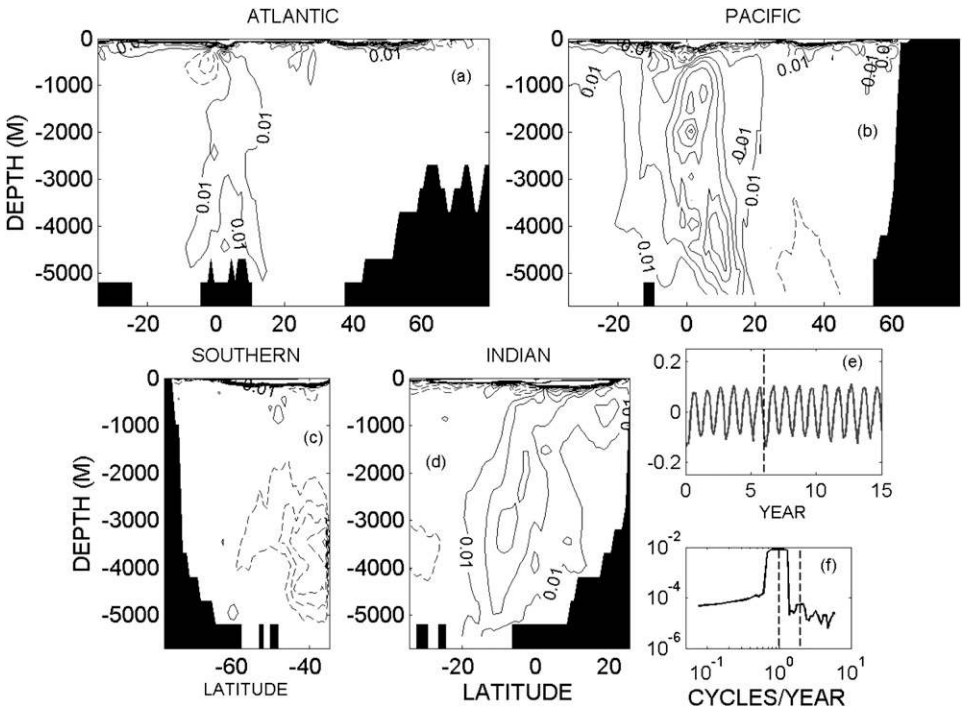

FIG. 9. (a)–(d) First global volume transport variability EOF (singular vector) $\mathbf{u}_1$, using monthly means, with about 44% of the total variance displayed in each ocean basin. Dashed contours are negative. This mode evidently represents the predominant and strong annual cycle in volume transport, and like most of the variability seen is largely tropical and dominated by the Pacific and Indian Oceans. Little North Atlantic response is visible (only contours with magnitude greater than or equal to 0.01 are shown). Consistent with linear theory, the Pacific response has a somewhat barotropic nature below the very surface layers. (e) The quantity $\mathbf{v}_1(t)$ and its power spectral density estimate, with the first 2 yr omitted from the analysis here and in the other plots. A hint of an ENSO response is visible (vertical dashed line in the plot of $\mathbf{v}_1$) in the 1997/98 transition time. (f) Vertical dashed lines on the spectral density of $\mathbf{v}_1(t)$ denote the annual and semiannual periods.

carry a slowly decreasing fraction of the variance and are dominated by the semiannual contributions.

Thus, a majority of the MOC variability is annual and, secondarily, semiannual; from the annual cycle to the decadal and larger time scale, it is dominated by the Pacific Ocean with its immense expanse of low-latitude, rapidly responsive volume; the low-latitude Indian Ocean is a close second in importance. That much greater volatility appears at low latitudes is consistent with the elementary Rossby wave theory sketched above. Although the ECCO–GODAE estimates are known to produce high-latitude convection that tends to penetrate too deeply owing to a failure to restratify rapidly enough, there is nonetheless only slight evidence for any annual variability at high latitudes from that effect. Many discussions exist of near-surface annual variability.

Rabe et al. (2008), for example, discuss the near-surface annual cycle in the tropical Atlantic from a 50-yr ECCO calculation, even though data prior to 1993 are extremely thin. Keenlyside and Kleeman (2002) summarize some of the theoretical understanding of the top about 200 m. The global decadal scale variability is not simple except insofar as it is dominated by low-latitude processes. Little or no high-latitude variability is evident. Jayne and Marotzke (2001) reviewed the entire subject of high-frequency enthalpy transport variations.

Dominance of the variability by the annual and semiannual cycles renders the higher-order EOFs unstable in terms of comparatively small residuals apart from those periods. To suppress this problem, the EOFs of the annual means of the records were computed. Of the total variance, all but about 13% is suppressed by the averaging. The first two EOFs of the residuals are displayed in Figs. 11 and 12 , which can be alternatively labeled the third and fourth EOFs or the first two of the annual means. The first of these, Fig. 11, shows a trendlike variability in the first years, flattening out toward the middle of the estimation period. In the North Atlantic (see Wunsch and Heimbach 2007), there is a mild weakening of the low-latitude transport in the

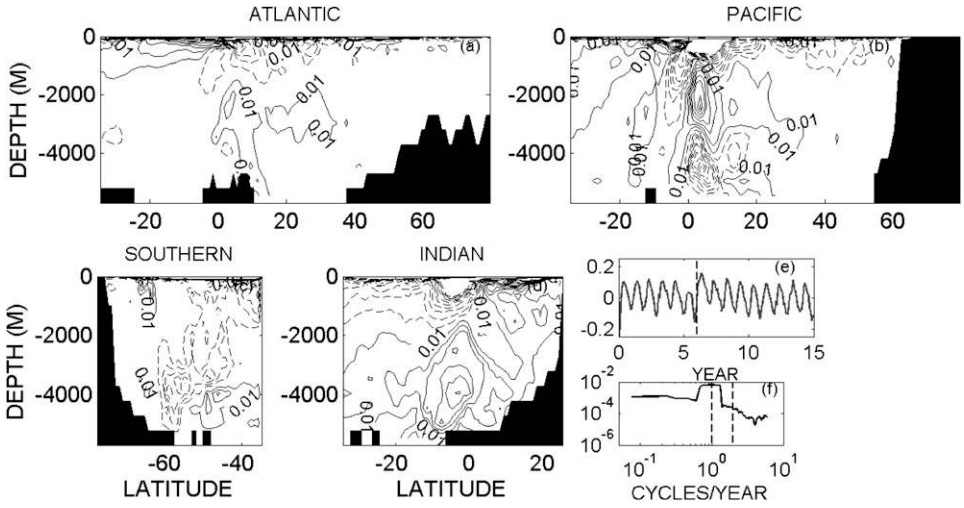

FIG. 10. As in Fig. 9, but for the second EOF of the meridional transport from monthly mean values with about 8% of the temporal variance. It is also dominantly annual in character but with a visible ENSO disturbance in the $\mathbf{v}_2(t)$ plot. Both the amplitude and phase recover quickly. Note incomplete contouring in the upper equatorial Pacific and Indian Oceans.

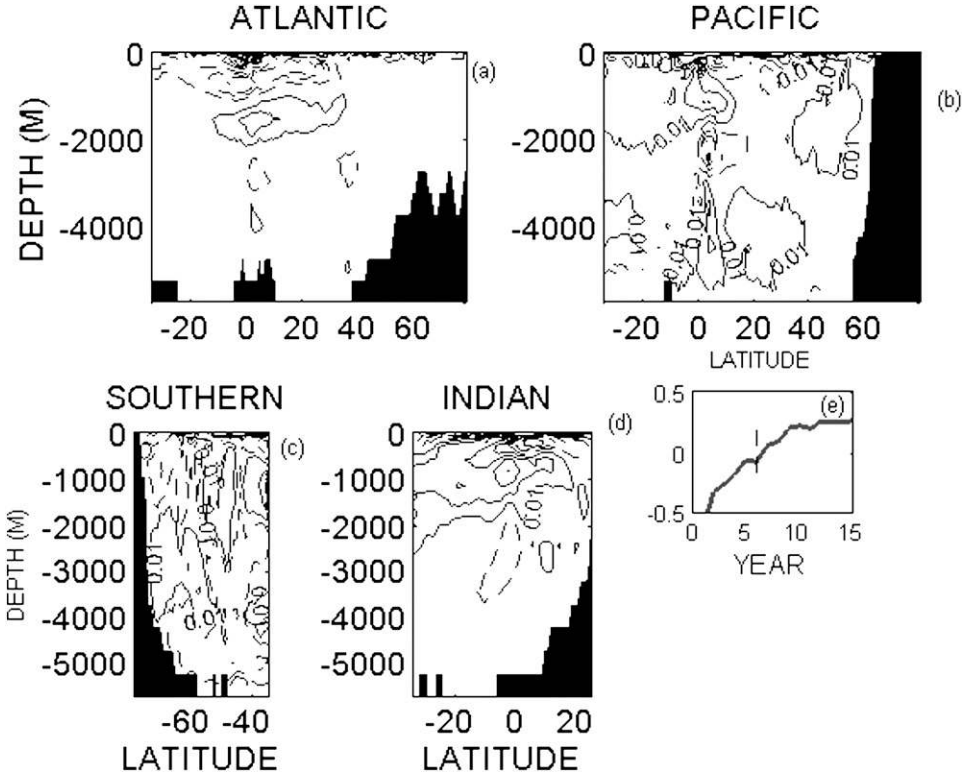

FIG. 11. First EOF of volume transport variability from *annual mean* values. This mode is trendlike over the first half of the estimation period, accounting for about 40% of the variability (which in turn is about 13% of the total variability based on monthly means). It is not easy to characterize the spatial structure. Panels are as in Fig. 9.

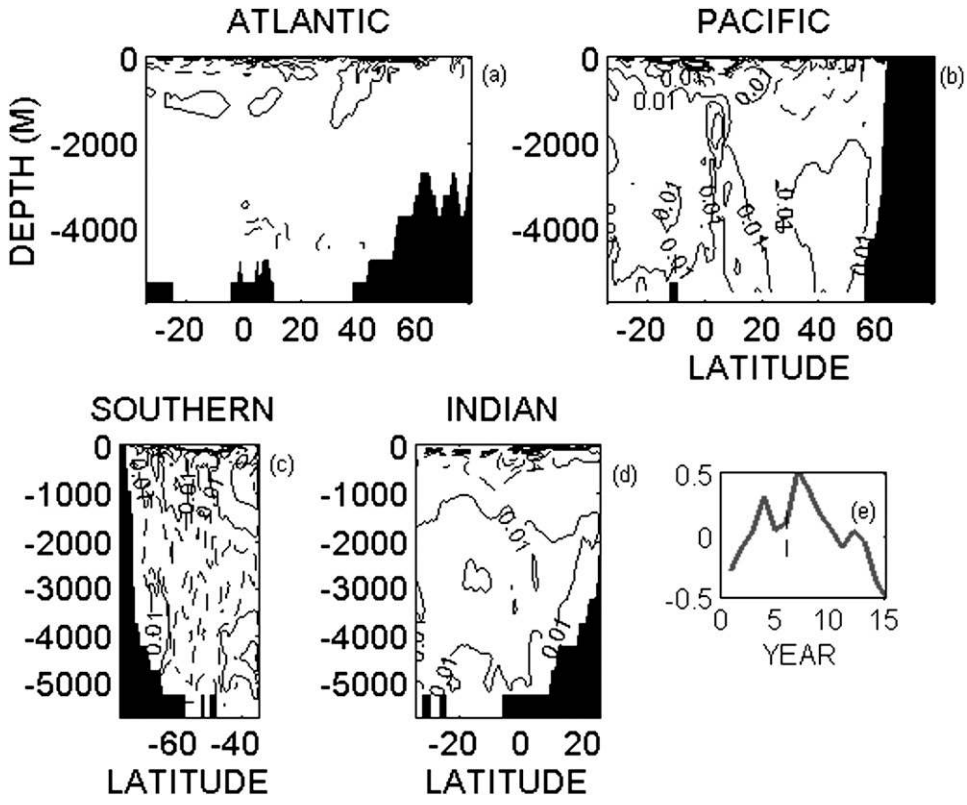

FIG. 12. Second EOF of the annual average transport variability, with about 15% of the variance at periods longer than the annual. A distinct change at the ENSO onset is seen in the time history.

upper ocean with a strengthening at depth. The rest of the World Ocean, particularly the Southern Ocean, displays an extremely complicated spatial pattern. This trendlike behavior will be briefly revisited below. The second annually averaged EOF defies a simple verbal description apart from the continued dominance in the Pacific and Indian Oceans of the low-latitude variability.

b. Temperature variability

The time-mean temperature (and salinity) fields are also visually conventional (a necessity forced by the least squares fit) and so are not displayed. The first variability EOF (whether from monthly mean or annual mean values) shows, exceptionally, a nearly linear trend in temperature over the entire calculated history (Fig. 13). It corresponds to a general warming everywhere and we will discuss it below. The major remaining temperature variability modes are annual and semiannual (not shown).

c. Enthalpy transports

About 20 EOFs are required to reproduce 95% of the squared norm of the variability. As with the volume flux, dominant variability is at the annual and semiannual periods (not shown) and mainly in the tropical Indian and Pacific Oceans.

The EOF in Fig. 14 from the annual means shows no obvious trend. As in the North Atlantic [as noted by Wunsch and Heimbach (2007)], the enthalpy transports display weaker apparent trends than do the volume fluxes, and to the degree that climate depends primarily on the former, there is no evidence after 15 yr for any major shift occurring in the global ocean circulation with climate consequences. That the enthalpy flux is not dominated by the trend seen in the first temperature EOF is consistent with inference of Wunsch and Heimbach (2006) for the North Atlantic, i.e. that the system is controlled by the variability in velocity, not in temperature, which is lost in the noise level.

4. Ice cover

Sea ice is an important component of the model at high latitudes, where observed ice cover is part of the misfit function. Its temporal variability (not shown) is primarily in the Southern Ocean annual cycle (with 92% of its temporal variance) and the semiannual one (5% of the variance). Higher EOFs are nearly white noise and

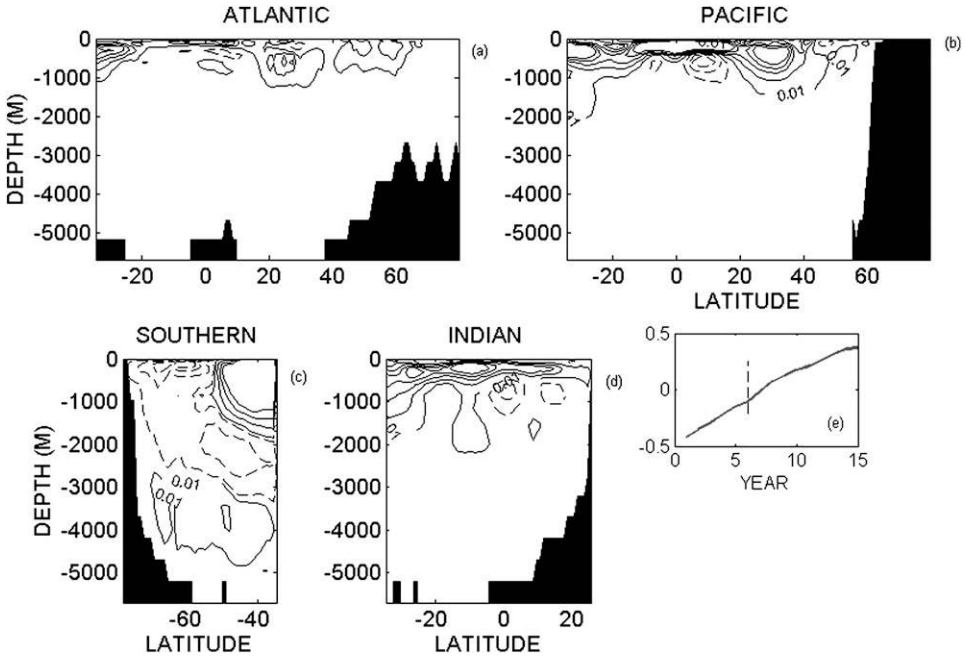

FIG. 13. First EOF of annual mean temperature field. This variability is dominated by an upper-ocean warming, attributable directly to the prior estimate from the meteorological reanalysis. It however appears to have little influence on the meridional enthalpy transport. The Southern Ocean, however, is a region of change in both signs. The EOF is essentially everywhere positive.

none of them suggests a sea ice-cover trend as seen in recent years in the Arctic. Note, however, that this system version does not include the Arctic itself.

5. The forcing

In the interests of comparative brevity, we discuss only the zonal wind component, which is much the stronger of the two. Time means of the meteorological forcing fields are not displayed here because they are visually unsurprising (e.g., with bands of easterlies and westerlies in the wind). Variability within the ocean can be the result of direct forcing structures, but it also arises from internal instabilities and free modes. Some insight can be gained by looking at the low EOFs of the forcing variables, with particular interest in any observed trends. Note in particular that much of the global-scale correlation structure seen in the oceanic

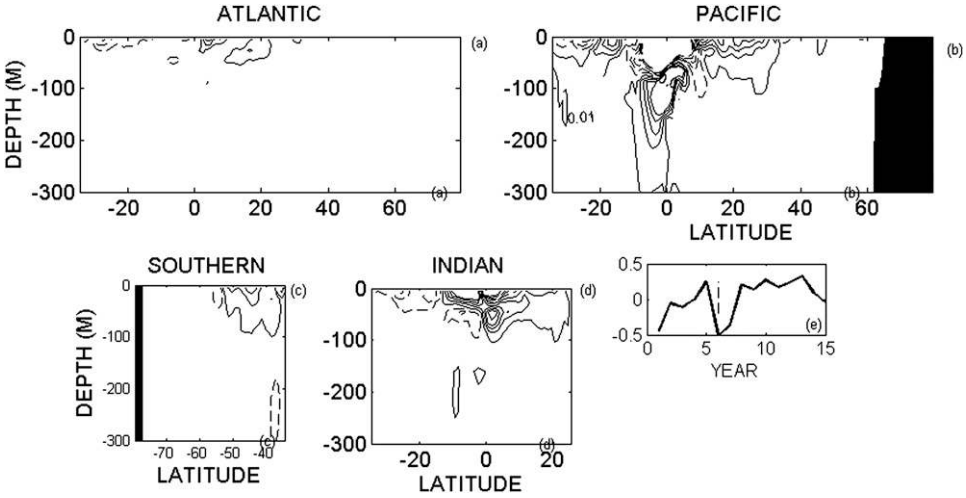

FIG. 14. First EOF (annual mean data) of the meridional enthalpy transport.

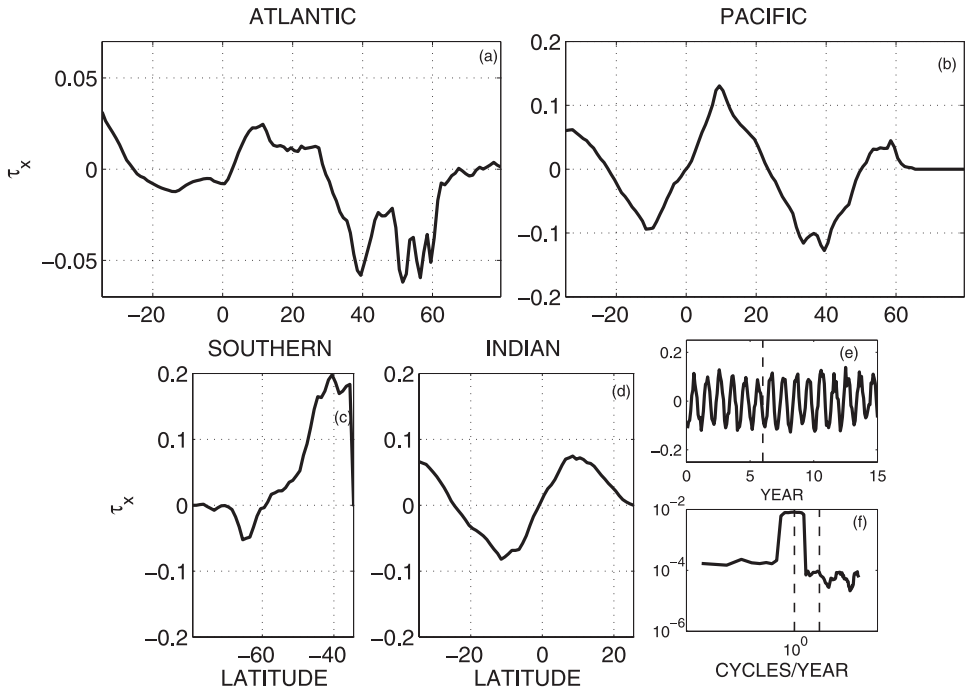

FIG. 15. First EOF, with about 39% of the variability in τ_x. It is essentially the annual variability and is dominated by the low-latitude Southern Ocean, with major contributions in the tropics (with the exception of the Atlantic). The Pacific and Indian Oceans have a remarkable near-perfect antisymmetry about the equator (vanishing there). Panels as in Fig. 9.

EOFs is most likely forced by the large-scale wind and buoyancy structures.

The first EOF of τ_x variability is shown in Fig. 15. This mode is essentially the annual variability and the second (not shown) is that of a broadband variability over the Arctic Circumpolar Current (ACC; Drake Passage latitude) with a separate semiannual peak. A strong semiannual peak in Southern Ocean winds is well known (e.g., Trenberth et al. 1990; Meehl 1991), as is another weak maximum in the North Pacific. Figure 16 displays the leading EOF of the annual average zonal wind. The strong Southern Ocean variability in this mode is sufficiently narrow in latitude that estimates (e.g., Cunningham and Pavic 2007) based on atmospheric pressure differences between 45° and 65°S would tend to miss the activity. A general discussion of atmospheric wind structures can be found in Thompson and Wallace (2000) and Thompson et al. (2000).

Huang et al. (2006) showed an apparent increase of 12% in the rate of working of the wind (as depicted by the NCEP–NCAR reanalysis) over the 25 yr beginning in 1980. To the extent that there exist trends in the zonal wind stress in the 15-yr period used here, they are a sum of spatially complicated structures in the higher EOFs (not shown). Figure 16e could be interpreted as showing an initial increase in the Southern Ocean zonal wind followed by a decrease toward the end of the estimation period.

A fundamental question is whether the meteorological disturbances applied to the ocean are sufficient to drive its response out of the range of the simple perturbation theory ideas invoked above. As we have seen, there is no particular evidence of long-term, large-scale trends that might be shifting the mean state, although surely low-frequency variability on time scales longer than 15 yr must be present. As a crude measure of the degree of disturbance, note that the space–time variance of the zonal stress is about 12% of the spatial variance of the time-mean field and includes the very strong annual cycle. There is no reason to believe that large-scale finite-amplitude responses are present now.

The first two EOFs of the enthalpy transfer to the atmosphere (not shown) have the same temporal structure as the wind field, but almost all of the variance is in the annual cycle with less than 1.5% in the semiannual (dominating the second EOF), which is again peaked over the Southern Ocean. No significant trends are observed.

6. The trends

Both the control and the present best estimate, v3.35, have an annual-mean temperature variability EOF

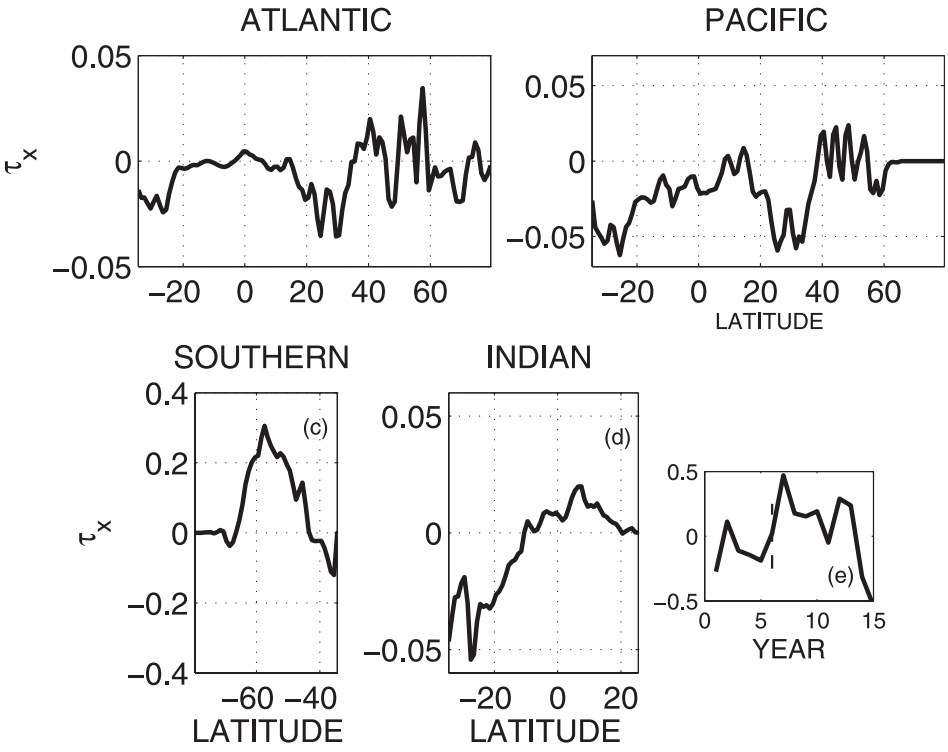

FIG. 16. First EOF of τ_x based on annual mean values of the adjusted wind field. The strong shift in the Southern Ocean has been noticed before, but it has much less energy than the annual cycle.

corresponding to a large-scale uptake of heat near the surface almost everywhere at a rate of about 3.4 W m^{-2}. This heating arises from the atmospheric state in the NCEP–NCAR reanalysis (Kalnay et al. 1996), which is derived from a weather forecast model now with global conservation constraints and employed here using bulk formulas. A value this large is implausible, and one would hope that there are adequate oceanic data on upper-layer temperatures and steric changes that would force its reduction. Although the value may well be reduced with further optimization iterations, there is no evidence that the oceanic data, within error bars, are in conflict with such a large heat uptake. The implication is that *oceanic data remain too sparse and noisy to force a reduction in the atmospheric heat flux.* Despite the presence of this injection of heat (whether real or not), has little or no effect on the meridional transports of volume (mass) or heat, being lost in the overall noisiness of the system. The wind field has already been discussed.

Bindoff et al. (2007) describe evidence for trends over several decades in oceanic ventilation rates through observations of such fields as the oxygen distribution. In the present 15-yr interval, the system is sufficiently noisy that whatever changes are taking place cannot be distinguished against the large interannual variability. Although it is possible that trends may become apparent over the much longer multidecadal span considered in the ventilation discussion, the extremely thin and poorly distributed in situ observations before the 1990s render unattainable the usefully accurate estimation of any global average [see the sampling discussion in the appendix of Wunsch et al. (2007)].

7. Discussion

Global solutions such as the ones used here describe a very large range of phenomena calling for details and explanation (keeping in mind the distortions implied by two-dimensional projections and the need to avoid interpreting the resulting Eulerian mean velocities as particle trajectories). We have touched on some of the more conspicuous fluctuations seen primarily in the tropics and the perhaps more surprising variability in the deep Southern Ocean, but without pursuing the details of either. The great bulk of the variability variance in the global MOC and its corresponding enthalpy transports over the 15-yr interval lies in the annual cycle, which at lowest order is consistent with the simplest expectations of linear Rossby wave dynamics [e.g., Gill and Niiler (1973), Jayne and Marotzke (2001), and Vinogradov et al. (2008) provide an extended

discussion of the annual cycle of variability in the state estimate used here]. This same theory strongly supports the inference that (absent finite-amplitude external forcing) multiple decades are required to detect deep ocean changes.

Basic theory shows that few or no large-scale baroclinic shifts are expected in the ocean over 15 yr, and no evidence has been found that the ocean has been or is undergoing any change sufficient to require moving beyond perturbation theory. The changes seen in the ECCO–GODAE estimate are small disturbances to the fully established general circulation, although the annual cycle forcing is always very large. Linear theory [Veronis and Stommel 1956; Pedlosky 2003; see Gill (1982) for a full account] shows that in the perturbation regime, large decadal changes in baroclinic structures are not expected outside of the tropics. Absent major changes in atmospheric forcing, which are also not seen, no sign exists of any significant trends or unusual behavior in the global MOC over the last 15 yr. What the future will bring is another question, but the implications of perturbation theory, the very large eddy noise present in the real system, and the enormous potential energy of the existing stratification all militate against the expectation of seeing major shifts on time scales shorter than many decades. Suggestions that the ocean circulation is or could be changing into radically different states need to address the energy sources required to make a qualitative change in the potential energy reservoirs.

What of the future? The dominant variability as seen here is annual and semiannual, consists of a few weak trends with complex spatial patterns, and has a long memory in the subsurface ocean. Anomalies propagating at depth in northern latitudes will require some decades to adjust the system and their presence is likely to produce some degree of local high-latitude predictability (persistence).[3] All of these inferences have strong implications for long-running circulation observation strategies, including the need to avoid aliasing of the strong seasonal cycles, to distinguish purely local effects from larger-scale ones, and to acquire the long duration of the observations that will be required for documentation and understanding.

The general linear theory of the prediction of stationary time series (Yaglom 1962) shows that more spectral structure produces longer prediction horizons. Thus, a narrowband annual cycle can be predicted accurately many years into the future. A general red noise process can be forecast with a skill dependent upon spectral steepness.

The stability of the annual cycle components, apart from the reaction of some singular vectors to the large ENSO signal of 1997–98, remains in keeping with the notion that only subtle changes have taken place in the ocean circulation since 1992.

Acknowledgments. Supported in part by the National Ocean Partnership Program (NOPP) with additional funding from the National Aeronautics and Space Administration. Computations were carried out at the National Center for Atmospheric Research (NSF funded), the Geophysical Fluid Dynamics Laboratory (NOAA), and elsewhere. Comments by M. Mazloff, A. Naveira Garabato, and two anonymous referees were helpful.

APPENDIX

EOFs and the Singular Value Decomposition

At a fixed time $t = t_p$, $\mathbf{v}'$ is a matrix with rows defining depths and columns defining latitude. For each such time, make a column vector of the matrix,

$$\mathbf{a}_p(t_p) = \text{vec}\,[\mathbf{V}'(\phi_j, z_k, t_p)],$$

and a new matrix $\mathbf{A}$ is defined by these columns:

$$\mathbf{A} = \{\mathbf{a}_p\}.$$

By the Eckart–Young–Mirsky theorem (e.g., Björck 1996, p. 12),

$$\mathbf{A} \approx \sum_{j=1}^{K} \lambda_j \mathbf{u}_j \mathbf{v}_j^{\mathrm{T}} \tag{A1}$$

gives the most efficient possible representation of $\mathbf{A}$ for any set of K orthonormal column vectors $\mathbf{u}_j$ and $\mathbf{v}_j$ if they are chosen as the singular vectors and λ_j are the singular values. (The $\mathbf{u}_j$ are commonly called the empirical orthogonal functions, a terminology we will use interchangeably, but the singular value decomposition form is more physically immediate.) The singular vectors $\mathbf{v}_j$ should not be confused with the meridional velocity component v. If $K = \min[M,N,\text{rank}(\mathbf{A})]$, then Eq. (A1) becomes an equality.

As always, the hope is that the required $K = K_{\text{eff}}$, the "effective" rank, is small. A simple measure of effectiveness is that $\sum_{j=1}^{K_{eff}} \lambda_j^2 / \sum_{j=1}^{K} \lambda_j^2$ represents the fraction of the variance of components of $\mathbf{A}$ described by Eq. (A1) measured as the square of the matrix Frobenius

[3] Hawkins and Sutton (2007) discuss the *much longer* time-scale variability of the global MOC within a coupled atmosphere–ocean model that is unconstrained by any observations.

norm of the difference of **A** from its singular value decomposition truncated at $j = K$. As has been widely recognized, in part because of the space–time orthogonality requirement, the singular vectors need not have a simple physical interpretation (although they may); rather, they are best regarded as an empirical, maximally efficient description of covariability in the fields.

The references (e.g., Jolliffe 2002; von Storch and Zwiers 1999) discuss the statistical reliability of these calculations. It is well known that the singular values are more robustly determined than are the corresponding singular vectors. Jolliffe (2002, pp. 42ff) provides approximate confidence intervals for both, and von Storch and Zwiers (1999, p. 303) discuss a useful simplification. In the present case, the λ_j have negligible uncertainty, but the EOF (singular vector) structures are unstable when the singular values are close to others. Thus, the discussion here is generally limited to the low-order terms corresponding to widely separated λ_i.

REFERENCES

Anderson, D. L. T., and R. A. Corry, 1985: Seasonal transport variations in the Florida Straits: A model study. *J. Phys. Oceanogr.,* **15,** 773–786.

Bindoff, N. L., and Coauthors, 2007: Observations: Oceanic climate change and sea level. *Climate Change 2007: The Physical Science Basis*, S. Solomon et al., Eds., Cambridge University Press, 386–432.

Björck, A., 1996: *Numerical Methods for Least Squares Problems*. SIAM, 408 pp.

Boccaletti, G., R. Ferrari, A. Adcroft, and J. Marshall, 2005: The vertical structure of ocean heat transport. *Geophys. Res. Lett.,* **32,** L10603, doi:10.1029/2005GL022474.

Cessi, P., K. Bryan, and R. Zhang, 2004: Global seiching of thermocline waters between the Atlantic and the Indian–Pacific Ocean basins. *Geophys. Res. Lett.,* **31,** L04302, doi:10.1029/2003GL019091.

Cunningham, S., and M. Pavic, 2007: Surface geostrophic currents across the Antarctic Circumpolar Current in Drake Passage from 1992 to 2004. *Prog. Oceanogr.,* **73,** 296–310.

Ferrari, R., and C. Wunsch, 2009: Ocean circulation kinetic energy—Reservoirs, sources and sinks. *Annu. Rev. Fluid Mech.,* **41,** 253–282.

Ganachaud, A., 2003: Large-scale mass transports, water mass formation, and diffusivities estimated from World Ocean Circulation Experiment (WOCE) hydrographic data. *J. Geophys. Res.,* **108,** 3213, doi:10.1029/2002JC001565.

——, and C. Wunsch, 2003: Large-scale ocean heat and freshwater transports during the World Ocean Circulation Experiment. *J. Climate,* **16,** 696–705.

Gill, A. E., 1982: *Atmosphere–Ocean Dynamics*. Academic Press, 662 pp.

——, and P. P. Niiler, 1973: The theory of the seasonal variability in the ocean. *Deep-Sea Res.,* **20,** 141–177.

Hawkins, E., and R. Sutton, 2007: Variability of the Atlantic thermohaline circulation described by three-dimensional empirical orthogonal functions. *Climate Dyn.,* **29,** 745–762.

Huang, R. X., W. Wang, and L. L. Liu, 2006: Decadal variability of wind-energy input to the world ocean. *Deep-Sea Res. II,* **53,** 31–41.

Hurrell, J. W., and Coauthors, 2006: Atlantic climate variability and predictability: CLIVAR perspective. *J. Climate,* **19,** 5100–5121.

Jayne, S. R., and J. Marotzke, 2001: The dynamics of ocean heat transport variability. *Rev. Geophys.,* **39,** 385–411.

Johnson, G. C., M. J. McPhaden, and E. Firing, 2001: Equatorial Pacific Ocean horizontal velocity, divergence, and upwelling. *J. Phys. Oceanogr.,* **31,** 839–849.

Jolliffe, I. T., 2002: *Principal Component Analysis*. 2nd ed. Springer, 487 pp.

Kalnay, E., and Coauthors, 1996: The NCEP/NCAR 40-Year Reanalysis Project. *Bull. Amer. Meteor. Soc.,* **77,** 437–471.

Keenlyside, N., and R. Kleeman, 2002: Annual cycle of equatorial zonal currents in the Pacific. *J. Geophys. Res.,* **107,** 3093, doi:10.1029/2000JC000711.

Lumpkin, R., and K. Speer, 2007: Global ocean meridional overturning. *J. Phys. Oceanogr.,* **37,** 2550–2562.

Mazloff, M., 2008: The southern ocean meridional overturning circulation as diagnosed from an eddy permitting state estimate. Ph.D. thesis, Massachusetts Institute of Technology/Woods Hole Oceanographic Institute, 125 pp.

Meehl, G. A., 1991: A reexamination of the mechanism of the semiannual oscillation in the Southern Hemisphere. *J. Climate,* **4,** 911–926.

Olbers, D., and K. Lettmann, 2007: Barotropic and baroclinic processes in the transport variability of the Antarctic Circumpolar Current. *Ocean Dyn.,* **57,** 559–578.

Pedlosky, J., 2003: *Waves in the Ocean and Atmosphere: Introduction to Wave Dynamics*. Springer, 250 pp.

Rabe, B., F. A. Schott, and A. Köhl, 2008: Mean circulation and variability of the tropical Atlantic during 1952–2001 in the GECCO assimilation fields. *J. Phys. Oceanogr.,* **38,** 177–192.

Scott, J. R., and J. Marotzke, 2002: The location of diapycnal mixing and the meridional overturning circulation. *J. Phys. Oceanogr.,* **32,** 3578–3595.

Sturges, W., B. G. Hong, and A. J. Clarke, 1998: Decadal wind forcing of the North Atlantic subtropical gyre. *J. Phys. Oceanogr.,* **28,** 659–668.

Talley, L. D., 2003: Shallow, intermediate, and deep overturning components of the global heat budget. *J. Phys. Oceanogr.,* **33,** 530–560.

Thompson, D. W. J., and J. M. Wallace, 2000: Annular modes in the extratropical circulation. Part I: Month-to-month variability. *J. Climate,* **13,** 1000–1016.

——, ——, and G. C. Hegerl, 2000: Annular modes in the extratropical circulation. Part II: Trends. *J. Climate,* **13,** 1018–1036.

Trenberth, K. E., W. G. Large, and J. G. Olson, 1990: The mean annual cycle in global ocean wind stress. *J. Phys. Oceanogr.,* **20,** 1742–1760.

Veronis, G., and H. Stommel, 1956: The action of variable wind stresses on a stratified ocean. *J. Mar. Res.,* **15,** 43–75.

Vinogradov, S. V., R. M. Ponte, P. Heimbach, and C. Wunsch, 2008: The mean seasonal cycle in sea level estimated from a data-constrained general circulation model. *J. Geophys. Res.,* **113,** C03032, doi:10.1029/2007JC004496.

VonStorch, H., and F. W. Zwiers, 1999: *Statistical Analysis in Climate Research*. Cambridge University Press, 484 pp.

Webb, D. J., and B. A. de Cuevas, 2007: On the fast response of the Southern Ocean to changes in the zonal wind. *Ocean Sci.,* **3,** 417–427.

Wunsch, C., 2005: The total meridional heat flux and its oceanic and atmospheric partition. *J. Climate,* **18,** 4374–4380.

——, 2008: Mass and volume transport variability in an eddy-filled ocean. *Nature Geosci.,* **1,** 165–168, doi:10.1038/ngeo126.

——, and P. Heimbach, 2006: Decadal changes in the North Atlantic meridional overturning and heat flux. *J. Phys. Oceanogr.,* **36,** 2012–2024.

——, and ——, 2007: Practical global oceanic state estimation. *Physica D,* **230,** 197–208.

——, and ——, 2008: How long to ocean tracer and proxy equilibrium? *Quat. Sci. Rev.,* **27,** 639–653.

——, R. Ponte, and P. Heimbach, 2007: Decadal trends in sea level patterns: 1993–2004. *J. Climate,* **20,** 5889–5991.

Yaglom, A. M., 1962: *An Introduction to the Theory of Stationary Random Functions.* Prentice Hall, 235 pp.